

## **NASA TECHNICAL MEMORANDUM 89153**

# **BEARING-BYPASS LOADING ON BOLTED COMPOSITE JOINTS**

(NASA-TM-89153) BEARING-BYPASS LOADING ON  
BOLTED COMPOSITE JOINTS (NASA) 34 p  
Avail: NTIS HC A03/MF A01 CSCL 11D

N87-25437

G3/24 Unclas  
0084707

**J. H. CREWS, JR. and R. A. NAIK**

**MAY 1987**

**NASA**

National Aeronautics and  
Space Administration

Langley Research Center  
Hampton, Virginia 23665

## SUMMARY

A combined experimental and analytical study has been conducted to investigate the effects of simultaneous bearing and bypass loading on a graphite/epoxy (T300/5208) laminate. Tests were conducted with a test machine that allows the bearing-bypass load ratio to be controlled while a single-fastener coupon is loaded to failure in either tension or compression. Test coupons consisted of 16-ply quasi-isotropic graphite/epoxy laminates with a centrally-located 6.35-mm bolt having a clearance fit. Onset-damage and ultimate strengths were determined for each test case. Next, a finite element stress analysis was conducted for each test case. The computed local stresses were used with appropriate failure criteria to analyze the observed failure modes and strengths. An unexpected interaction of the effect of the bypass and bearing loads was found for the onset of compression-reacted bearing damage. This interaction was caused by a decrease in the bolt-hole contact arc and a corresponding increase in the severity of the bearing loads. The amount of bolt-hole contact had a significant effect on local stresses and, thus, on the calculated damage-onset and ultimate strengths. An offset-compression failure mode was identified for laminate failure under compression bearing-bypass loading. This failure mode appears to be unique to compression bearing-bypass loading and, therefore, cannot be predicted from simple tests.

## INTRODUCTION

In the past, composite joints have often been designed using rather simple metals-based procedures without encountering serious problems. In most such cases, the structural design strains have been limited by damage-tolerance considerations, and at low structural strain levels, the joints have been adequate. However, as tougher composites come into use, the design strains will rise and structural joining requirements will become more critical. Analytical design procedures for joints should be based on a sound understanding of the response of composite materials under loading conditions similar to those in multi-fastener joints.

Within multi-fastener joints, fastener holes may be subjected to both bearing loads and loads that bypass the hole, as shown in figure 1. The ratio of the bearing load to the bypass load depends on the joint stiffness and configuration. As the joint is loaded, this bearing-bypass ratio at each fastener remains nearly constant until damage begins to develop. In general, different bearing-bypass ratios produce different failure modes and strengths for each fastener hole. The laminate response can be studied by testing single-fastener specimens under bearing-bypass loading, but such tests are usually difficult. The first objective of the present paper is to describe a relatively simple approach for the bearing-bypass testing of single-fastener coupons. This approach uses two hydraulic servo-control systems to apply proportional bearing and bypass loads to a specimen with a central hole. The second objective of this paper is to present bearing-bypass strength data for a wide range of bearing-bypass ratios in both tension and compression. Previous data in the

literature have been rather limited, especially for compression. The test specimens were made of T300/5208 graphite/epoxy in a 16-ply quasi-isotropic layup. The bearing loads were applied through a clearance-fit steel bolt having a nominal diameter of 6.35 mm. The test results are presented as bearing-bypass diagrams for damage-onset strength and for ultimate strength. The corresponding damage modes were determined by radiographing each specimen after testing.

The third objective of this study was the analysis of the bearing-bypass test results using the local stresses around the bolt hole, computed for combined bearing and bypass loading. These stresses were calculated using a finite element procedure that accounted for nonlinear bolt-hole contact. The corresponding contact angles were calculated, as well as the local stress distributions. The stresses were used to compute the damage-onset and ultimate strengths for the range of bearing-bypass test conditions. The computed strengths were used to discuss the test trends.

#### NOMENCLATURE

$C$	bolt-hole clearance, m
$d$	hole diameter, m
$P_a$	applied load, N
$P_b$	bearing load, N
$P_p$	bypass load, N
$S_b$	nominal bearing stress, MPa
$S_{np}$	nominal net-section bypass stress, MPa
$r, \theta$	polar coordinates, m, deg

$t$	specimen thickness, m
$w$	specimen width, m
$x, y$	Cartesian coordinates, m
$\beta$	bearing-bypass ratio
$\theta_1$	bolt-hole contact half-angle for single contact, deg
$\theta_2$	secondary bolt-hole contact half-angle for dual contact, deg
$\sigma_{rr}$	radial stress component, MPa
$\sigma_{\theta\theta}$	tangential stress component, MPa

## BEARING BYPASS TESTING

### Test Procedure

The test specimen configuration and loading combinations are shown in figure 2. The graphite/epoxy specimens were machined from a single  $[0/45/90/-45]_{2s}$  panel. The bolt holes were machined using an ultrasonic diamond core drill. They were then carefully hand-reamed to produce a clearance of 0.076 mm with the steel bolts. This clearance, 1.2 percent of the hole diameter, is typical of aircraft joints.

The test system used in this study is shown schematically in figure 3. The center of the specimen is bolted between two bearing-reaction plates that are attached to the load frame using two load cells. The ends of the specimen are then gripped and loaded independently by two servo-control systems (called "upper" and "lower" in figure 3). Any difference between these two end loads produces a bearing load at the central bolt hole. This bearing load is measured

by the load cells under the bearing-reaction plates. The end loads are synchronized by a common input signal; as a result, a constant bearing-bypass ratio is maintained throughout each test.

A photograph of the apparatus is shown in figure 4. This photograph shows the friction grips that load each end of the specimen and the head of the steel bolt that attaches the specimen to the bearing-reaction plates. Only a small portion of the specimen edge is visible. Notice that the bearing-reaction plates are bolted to the bearing load cells, allowing either tension or compression bearing loads. During compression, the bearing-reaction plates prevent specimen buckling. Although not visible in this photograph, hardened steel bushings were used between the bolt and the bearing-reaction plates. These 12.7-mm bushings were machined for a sliding fit, allowing the bolt clamp-up force to be transmitted to the local region around the bolt hole. This arrangement was equivalent to having a clamp-up washer directly against the side of the specimen, as was used in references 1, 2, and 3. For the present tests, the bolt was finger tightened (about 0.2 Nm torque) to produce a very small clamp-up force against the specimen.

The loading notations for tension and compression testing are shown in figure 2(b). All tests were conducted at a rather slow loading rate of 3.75 N/s. The results are reported in terms of nominal bearing stress  $S_b$  and nominal net-section bypass stress  $S_{np}$ , calculated using the following equations:

$$S_b = P_b / td$$

$$S_{np} = P_p / t (w - d)$$

where  $t$  is specimen thickness and  $w$  is the width. The bearing-bypass ratio  $\beta$  is defined as

$$\beta = S_b / S_{np}$$

Throughout each test, the specimen deformation was measured by displacement transducers. These transducers were mounted symmetrically on the front and back of the bearing-reaction plates, see figure 4. (These plates were made from nonmagnetic 347 stainless steel so they would not affect the transducers.) The transducer rods rested on small bars that were cemented to the specimen slightly above the grip line. This arrangement provided a measurement of the relative displacement between the bearing-reaction plates and the specimen. These measurements were used to determine the onset of damage.

The bearing and bypass loads were plotted against the specimen displacement, shown for a typical case in figure 5. Both the bearing and bypass curves have a small initial nonlinearity (probably due to varying bolt-hole contact) but gradually develop a nearly linear response. At higher load levels, the curves gradually develop a second nonlinearity, which indicates damage at the bolt hole, as mentioned in reference 3. An offset of  $0.001d$  was selected to define the damage-onset load, as indicated in figure 5. Some specimens were unloaded after the damage-onset load level and were then treated with an X-ray opaque dye-penetrant and radiographed to determine the damage-onset mode.

### Test Results

Figure 6 shows radiographs of four damage-onset modes. For tension dominated loading, the damage developed in the net-section tension (NT) mode,

figure 6(a). The gray shadows show delaminations and the dark bands indicate ply splits. The tension-reacted bearing (TRB) and compression-reacted bearing (CRB) damage modes are quite similar, as expected, and appear to be delamination dominated. The net-section compression (NC) mode involves rather discrete damage zones extending from the hole. This damage was probably caused by microbuckling in the  $0^{\circ}$  plies.

The measured  $S_b$  and  $S_{np}$  values corresponding to damage onset are plotted against one another in figure 7, as a so-called bearing-bypass diagram. Each open symbol represents the average of three tests and the tick marks indicate the range of the measured strengths, plotted along lines of constant  $\beta$ . The data in figure 7, also given in Table 1, were taken from reference 4. The right side of figure 7 shows tension results for four  $\beta$  values (0, 1, 3,  $\infty$ ). The symbol on the  $S_{np}$  axis represents the all bypass loading in tension ( $\beta = 0$ ). The NT next to the symbol indicates net-section tension damage. As expected, all the test cases with NT damage can be represented by a straight line and, thus, show the linear interaction discussed in references 3 and 5. This linearity suggests that the local stresses due to bearing loading and those due to bypass loading each contribute directly to failure. The "bearing-cutoff" line was drawn through the  $\beta = \infty$  data point. The damage-onset strengths for the all bearing tension case ( $\beta = \infty$ ) and the all bearing compression case ( $\beta = -\infty$ ) differ by about three percent. However, the bearing-cutoff line used for tension does not appear to apply for compression. The CRB damage mode was found at  $\beta = -1$  for a much lower strength level. The compressive bypass load had a somewhat unexpected effect on the onset of bearing damage. The bearing failure for combined bearing and bypass loading was analyzed in reference 3 and resulted from a decrease in the bolt-hole contact angle caused by the

compressive bypass load. For the all bypass compressive loading ( $\beta = -0$ ), NC damage initiated at -422 MPa, which is much larger than the expected compression strength for this laminate. This suggests that "dual" bolt-hole contact developed, allowing the load to transfer across the hole, and, therefore, produced a higher strength. This will be discussed later in an analysis of the bolt-hole contact.

The bearing-bypass diagram for the ultimate strengths (solid symbols) is shown in figure 8. To evaluate the progression of damage from onset to ultimate failure, the damage-onset curves are replotted from figure 7. A general comparison of these two sets of results shows that the specimens failed immediately after damage onset when an all bypass loading ( $\beta = 0$  and  $-0$ ) was used. In contrast, for the all bearing loading ( $\beta = \infty$  and  $-\infty$ ), the specimens failed at considerably higher loads than required to initiate damage. Also, when bearing and bypass loads were combined, the specimens showed additional strength after damage onset, more so in compression. A comparison of the damage modes indicated in figure 8 shows that the onset-damage mode was the ultimate failure mode in most cases. The exception occurred for the compressive bearing-bypass loading. For  $\beta = -3$ , the damage initiated in the CRB mode but the specimen failed in a different mode, referred to here as the offset-compression (OSC) mode. Figure 9 shows a specimen that failed in the OSC mode. The failure is typical of a compression failure but developed away from the specimen net-section. The light region near the fracture is a solid film lubricant that transferred from the bearing-reaction plate when the specimen failed. The offset of the failure from the net section is believed to be caused by the CRB delamination damage extending beyond the clamp-up area around the hole, thereby initiating a compression failure away from the hole. This transition from the

CRB damage-onset mode to the OSC failure mode could also happen in multi-fastener joints and, therefore, may be an additional complication when joint strength predictions are made for compressive loadings.

## STRESS ANALYSIS

In this section, first, the stress analysis procedures are briefly described. Then, stresses at the hole boundary are shown for selected combinations of bearing-bypass loading in tension and compression. These stress results are then used in the next section to calculate the specimen strengths for the various damage modes observed in the bearing-bypass tests.

### Finite Element Procedures

The finite element procedures used in this study were presented and evaluated in reference 6. When a bolt clearance is used, as in the present study, the contact angle at the bolt-hole interface varies with applied load, as shown in figure 10. Using the inverse technique described in reference 6, this nonlinear problem is reduced to a linear problem. In this technique, for a simple bearing loading, a contact angle is assumed and the corresponding bearing load is calculated. This procedure is repeated for a range of contact angles to establish a relationship between contact angle and bearing load. In the present study, this technique was extended to include combined bearing and bypass loading. For each bearing-bypass ratio  $\beta$ , the combined bearing and bypass loading was expressed in terms of bearing stress  $S_b$  and  $\beta$ . Thus, for a given  $\beta$ , the procedure was identical to that used in reference 6. This procedure was

repeated to establish a relationship between contact angle and bearing-bypass loading for each  $\beta$  value in the test program.

These calculations were done using the NASTRAN finite element code. This code is well suited for the inverse technique because the contact of the bolt and the hole can be represented using displacement constraints along a portion of the hole boundary. Displaced nodes on the hole boundary were constrained to lie on a circular arc corresponding to the bolt surface. This represent a rigid bolt having a frictionless interface with the hole. A very fine two-dimensional mesh was used to model the test specimen. Along the hole boundary, elements subtended less than  $1^\circ$  of arc. As a result, the contact arc could be modeled very accurately.

#### Stress Results

Figure 11 shows the hole-boundary stress distributions for three tension loading cases. The first case is an all bypass tension loading ( $\beta = 0$ ); the hole-boundary tangential stress  $\sigma_{\theta\theta}$  is shown as a dash-dot curve. It has the expected peak at  $\theta = 90^\circ$ , the specimen net-section. The value of this  $\sigma_{\theta\theta}$  peak can be used to predict the applied load for damage onset in the NT mode, as demonstrated in reference 2. The second case in figure 11 represents an all bearing tension loading ( $\beta = \infty$ ) of 400 MPa with zero clearance between the bolt and the hole;  $\sigma_{\theta\theta}$  and  $\sigma_{rr}$  are shown as dashed curves. The peak value of the  $\sigma_{rr}$  curve governs the bearing damage onset. The  $\sigma_{rr}$  curve also indicates a contact angle of about  $82^\circ$ ; the peak value in the  $\sigma_{\theta\theta}$  curve occurs slightly beyond the end of the contact angle. The third case in figure 11, the solid

curves, also represents an all bearing case with  $S_b = 400$  MPa, but with the 0.076 mm clearance used in the tests. Comparison of the  $\sigma_{rr}$  curves for the two all bearing cases shows that the clearance reduced the contact angle by about  $20^\circ$  and increased the  $\sigma_{rr}$  bearing stress. Thus, clearance tends to decrease bearing strength.

Hole-boundary stresses for tension bearing-bypass loading are shown in figure 12. These results correspond to a bearing stress  $S_b$  of 400 MPa with three tension bypass stress  $S_{np}$  levels. The  $\sigma_{rr}$  curves show that increasing  $S_{np}$ , the bypass load, caused the contact angle to increase. However, the peak  $\sigma_{rr}$  value changed very little for increasing  $S_{np}$ , suggesting that tension bypass loading has little influence on the bearing strength. In contrast, increasing the tension bypass stress levels produced higher  $\sigma_{\theta\theta}$  peaks, which corresponds to lower net-section tension strengths.

Hole-boundary stresses for compression bearing-bypass loading are shown in figure 13. Again, the bearing stress  $S_b$  was 400 MPa. The  $\sigma_{rr}$  curves show that increasing the compressive  $S_{np}$  value produced smaller contact angles and correspondingly higher peak  $\sigma_{rr}$  values. This shows that the value of  $S_{np}$  influences the bearing strength, as shown previously in figure 7. The  $\sigma_{\theta\theta}$  tensile peaks were nearly the same for the range of  $S_{np}$  values but the  $\sigma_{rr}$  compressive peaks varied widely. The curve for  $S_{np} = 500$  MPa illustrates dual contact; notice the  $\sigma_{rr}$  contact stress near  $\theta = 180^\circ$ .

The contact angle trends discussed in figures 12 and 13 are summarized in figure 14. The contact angles,  $\theta_1$  and  $\theta_2$  defined by the insert, are

shown for a range of tension and compression bypass loadings with  $S_b = 400$  MPa. Increasing the tensile bypass loading increased  $\theta_1$ , while increasing the compressive bypass loading had the opposite effect. The small jog in the curve at  $S_{np} = 0$  is caused by the small difference between tension-reacted bearing and compression-reacted bearing. Notice that dual contact initiated for a compressive bypass stress of about 450 MPa. The secondary contact angle  $\theta_2$  increased rather abruptly as the compressive  $S_{np}$  exceeded this value. Additionally, the decreasing trend for  $\theta_1$  reversed when dual contact developed. Dual contact provides a path for the applied load to "bridge" across the hole rather than divert around it. This reduces the stress concentration in the net section and produces higher net-section compression strength than with no dual contact.

#### STRENGTH CALCULATIONS

As previously mentioned, laminate strengths for bearing-bypass loading were calculated using the local stresses at the bolt hole. These calculations were used to study the strength trends for the range of loading combinations and the different failure modes. The damage-onset strengths were calculated using the peak hole-boundary stresses, as in reference 2. The onset of damage was assumed to occur when the peak hole-boundary stress reached a critical value for each damage mode. For each measured damage-onset strength, the peak stress was calculated and the average of the peaks in each damage mode was assumed to be the critical value for that damage mode. The following critical values were calculated for each damage mode: 869 MPa for NT; -760 MPa for TRB; -808 MPa for

CRB; and -817 MPa for NC. The solid curves in figure 15 represent the damage-onset strengths calculated in this manner. The average damage-onset strength data from figure 7 are replotted as open symbols in figure 15. The calculated curves agree with the data trends for strength. Also, the calculated damage modes agree with those discussed earlier. This demonstrates that damage-onset strengths can be predicted from the peak hole-boundary stresses if a critical stress value is known for each damage mode.

The ultimate strengths for bearing-bypass loading were calculated using the well-known point-stress criterion (reference 7). The stress distribution calculated along the observed direction of damage growth near the hole was compared with the laminate strength to determine a characteristic dimension. This failure theory was fit to the test data for each failure mode to determine an average characteristic dimension. As explained in reference 4, the following characteristic dimensions were determined for each failure mode: 2.44 mm for NT; 2.22 mm for TRB; 3.87 mm for CRB; 8.89 mm for OSC; and 2.54 mm for NC. The strength calculations must agree with the data averages for each failure mode. As expected, the calculations also agreed with the trends for the strength data, as shown by the dash-dot curves and solid symbols in figure 15.

The correlation between the strength calculations and the strength measurements in figure 15 suggests that a combined analytical and experimental approach could be used to predict bearing-bypass diagrams from a few tests. Such tests could be conducted for the all bypass ( $\beta = 0$ ) and the all bearing ( $\beta = \infty$ ) cases to determine the critical material strength parameters, which could then be used with a stress analysis to construct curves for the more complicated cases of bearing-bypass loading. This approach seems viable for tension bearing-bypass loading because only two failure modes are involved. But for compression loading, there are three ultimate failure modes. The OSC mode

occurs only for combined bearing and bypass loading, so this failure mode cannot be evaluated using simple loading. Therefore, strength calculations for compression would require bearing-bypass tests for at least one  $\beta$  value to find the OSC material strength parameter.

#### CONCLUDING REMARKS

A combined experimental and analytical study has been conducted to investigate the effects of combined bearing and bypass loading on a graphite/epoxy (T300/5208) laminate. Tests were conducted on single-fastener specimens loaded in either tension or compression. Test specimens consisted of 16-ply, quasi-isotropic graphite/epoxy laminates with a centrally-located hole. Bearing loads were applied through a steel bolt having a clearance fit. Onset damage, ultimate strengths, and the corresponding failure modes were determined for each test case. A finite element procedure was used to calculate the local stresses around the bolt hole.

A dual-control test system, described in this paper, was used to successfully measure laminate strengths for a wide range of bearing-bypass load ratios in both tension and compression. The tension data showed the expected linear interaction for combined bearing and bypass loading where the damage developed in the net-section tension mode. However, the bearing damage-onset strengths in compression showed an unexpected interaction of the effects for the bearing and bypass loads. Compressive bypass loads reduced the bearing onset strength. The compressive bypass loading decreased the bolt-hole contact arc, which increased the severity of the compressive bearing loads. Compressive

bearing-bypass loading also produced an off-set compression (OSC) failure mode, not previously reported in the literature.

The present stress analyses showed that combined bearing and bypass loading can have a significant influence on the bolt-hole contact angles. These contact angles had a strong influence on the local stresses around the hole; they must, therefore, be accurately represented in strength calculation procedures that are based on local stresses.

Although the trends in the bolt-hole strength for combined bearing and bypass loading were accurately calculated using local stresses together with failure criteria, some bearing-bypass testing is required to predict the compression response. The laminate response under compression bearing-bypass loading involved the OSC failure mode, which cannot be evaluated by simple loading conditions. Therefore, predictions of laminate bearing-bypass strengths may need to be combined with selected bearing-bypass testing to account for the off-set compression failure mode.

## REFERENCES

1. Crews, J. H., Jr.: "Bolt-Bearing Fatigue of a Graphite/Epoxy Laminate," *Joining of Composite Materials*, ASTM STP 749, K. T. Kedward, Ed., American Society for Testing and Materials, 1981, pp. 131-144.
2. Crews, J. H., Jr. and Naik, R. A.: "Failure Analysis of a Graphite/Epoxy Laminate Subjected to Bolt-Bearing Loads," *Composite Materials: Fatigue and Fracture*, ASTM STP 907, H. T. Hahn, Ed., American Society for Testing and Materials, 1986, pp. 115-133.
3. Crews, J. H., Jr. and Naik, R. A.: "Combined Bearing and Bypass Loading on a Graphite/Epoxy Laminate," *Composite Structures*, Vol. 6, 1986, pp. 21-40.
4. Naik, R. A.: "An Analytical and Experimental Study of Clearance and Bearing-Bypass Load Effects in Composite Bolted Joints," Ph.D. dissertation, Old Dominion University, Norfolk, Virginia, August 1986.
5. Hart-Smith, L. J.: "Bolted Joints in Graphite/Epoxy Composites, NASA CR-144899, National Aeronautics and Space Administration, January 1977.
6. Naik, R. A. and Crews, J. H. Jr.: "Stress Analysis Method for a Clearance-Fit Bolt under Bearing Loads," *AIAA Journal*, Vol. 24, No. 8, August 1986, pp. 1348-1353.
7. Whitney, J. M. and Nuismer, R. J.: "Stress Fracture Criteria for Laminated Composites Containing Stress Concentrations," *J. Composite Materials*, Vol. 8, July 1974, pp. 253-265.

**Table 1     Laminate strengths for bearing-bypass loading.**

Bearing- bypass ratio, $\beta$	Damage-Onset			Ultimate Failure		
	$S_b$ (MPa)	$S_{np}$ (MPa)	Mode	$S_b$ (MPa)	$S_{np}$ (MPa)	Mode
<u>Tension</u>						
0	0	304	NT	0	330	NT
1	237	237	NT	263	263	NT
3	468	156	NT	648	216	NT
$\infty$	542	0	TRB	812	0	TRB
<u>Compression</u>						
-0	0	-422	NC	0	-422	NC
-1	314	-314	CRB/NC	461	-461	OSC
-3	498	-166	CRB	759	-253	OSC
$-\infty$	528	0	CRB	853	0	CRB

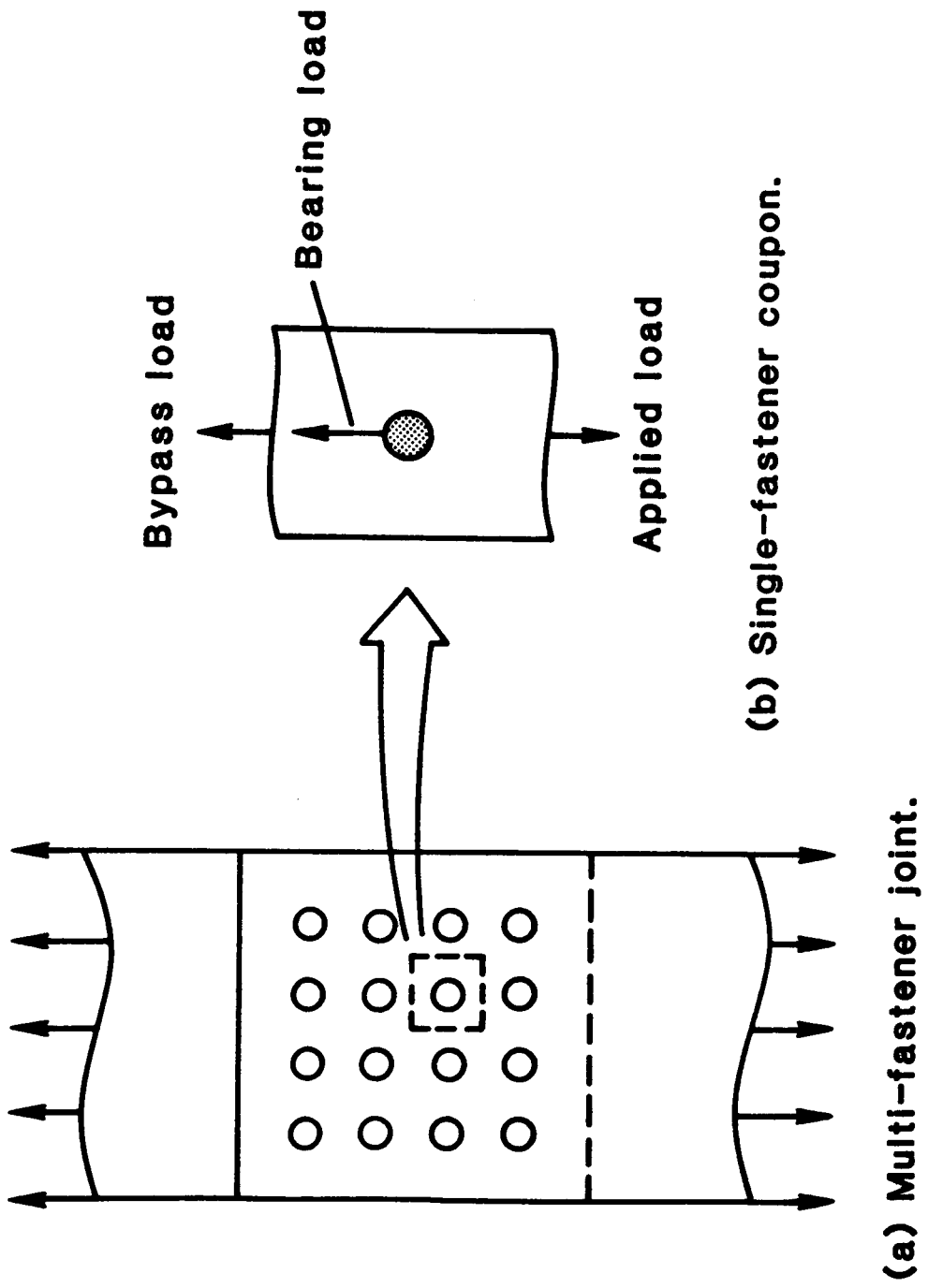


Figure 1 Bearing-bypass loading within a multi-fastener joint.

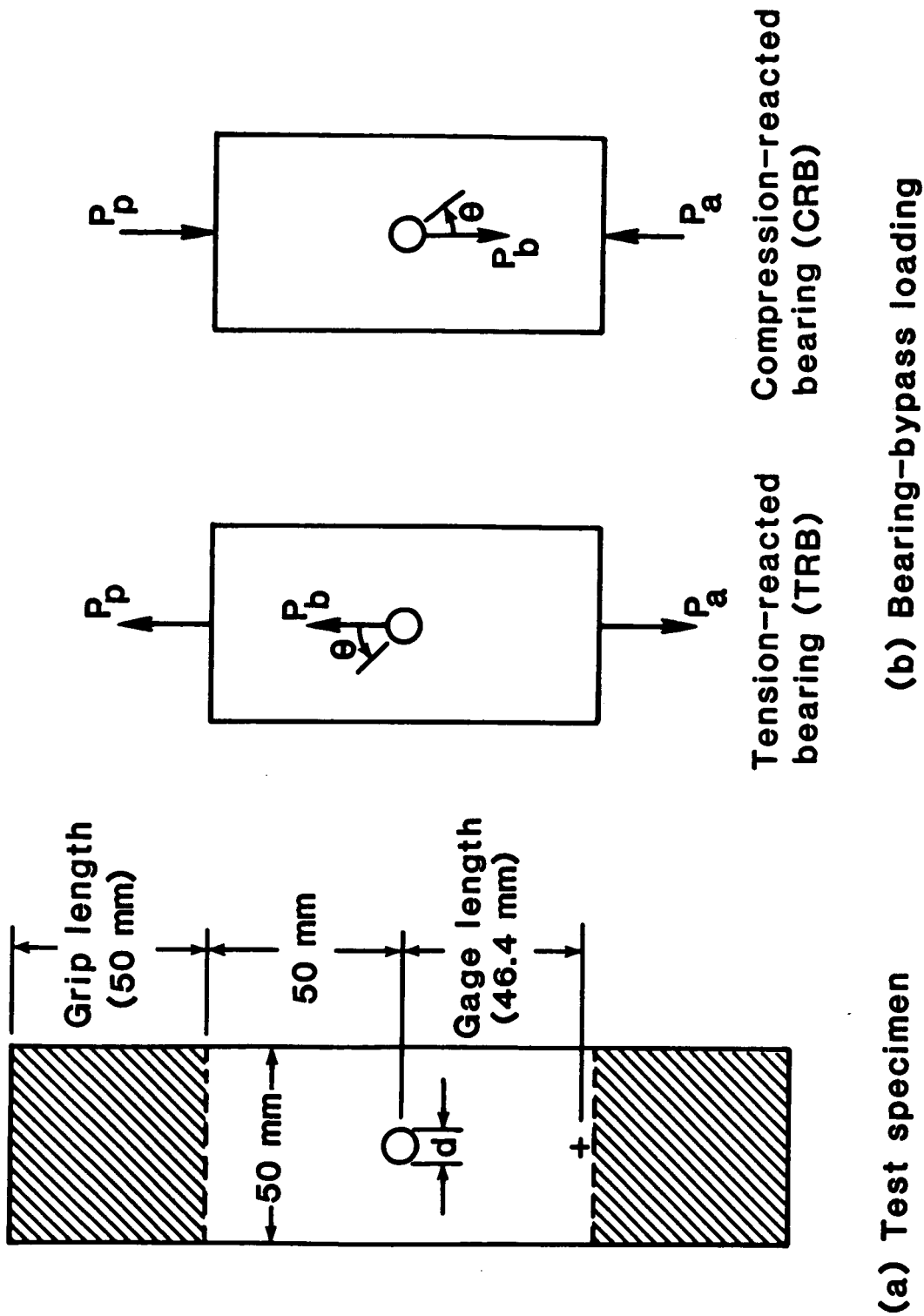


Figure 2 Specimen configuration and bearing-bypass loading.

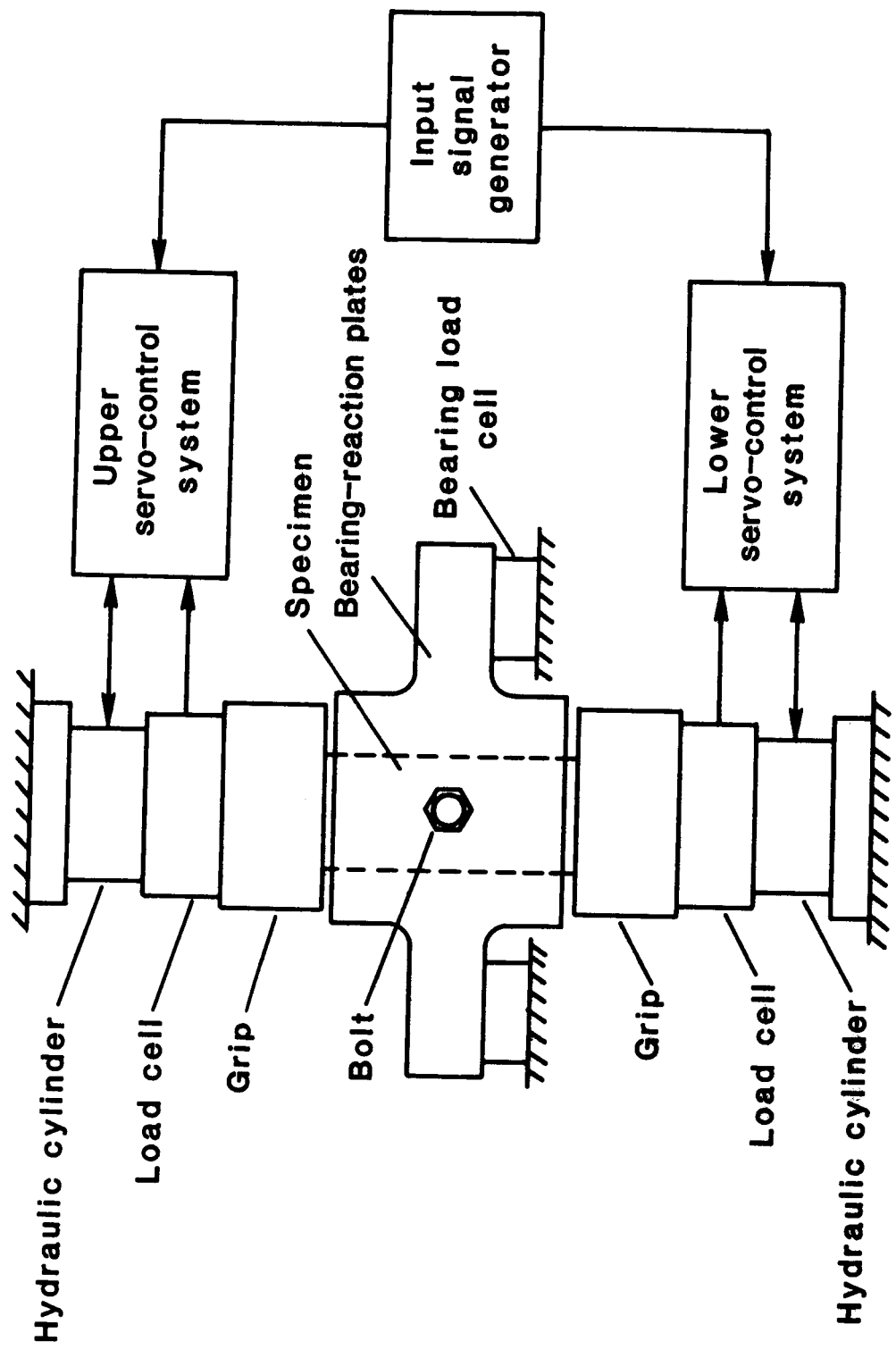


Figure 3 Block diagram of the bearing-bypass test system.

ORIGINAL PAGE IS  
OF POOR QUALITY

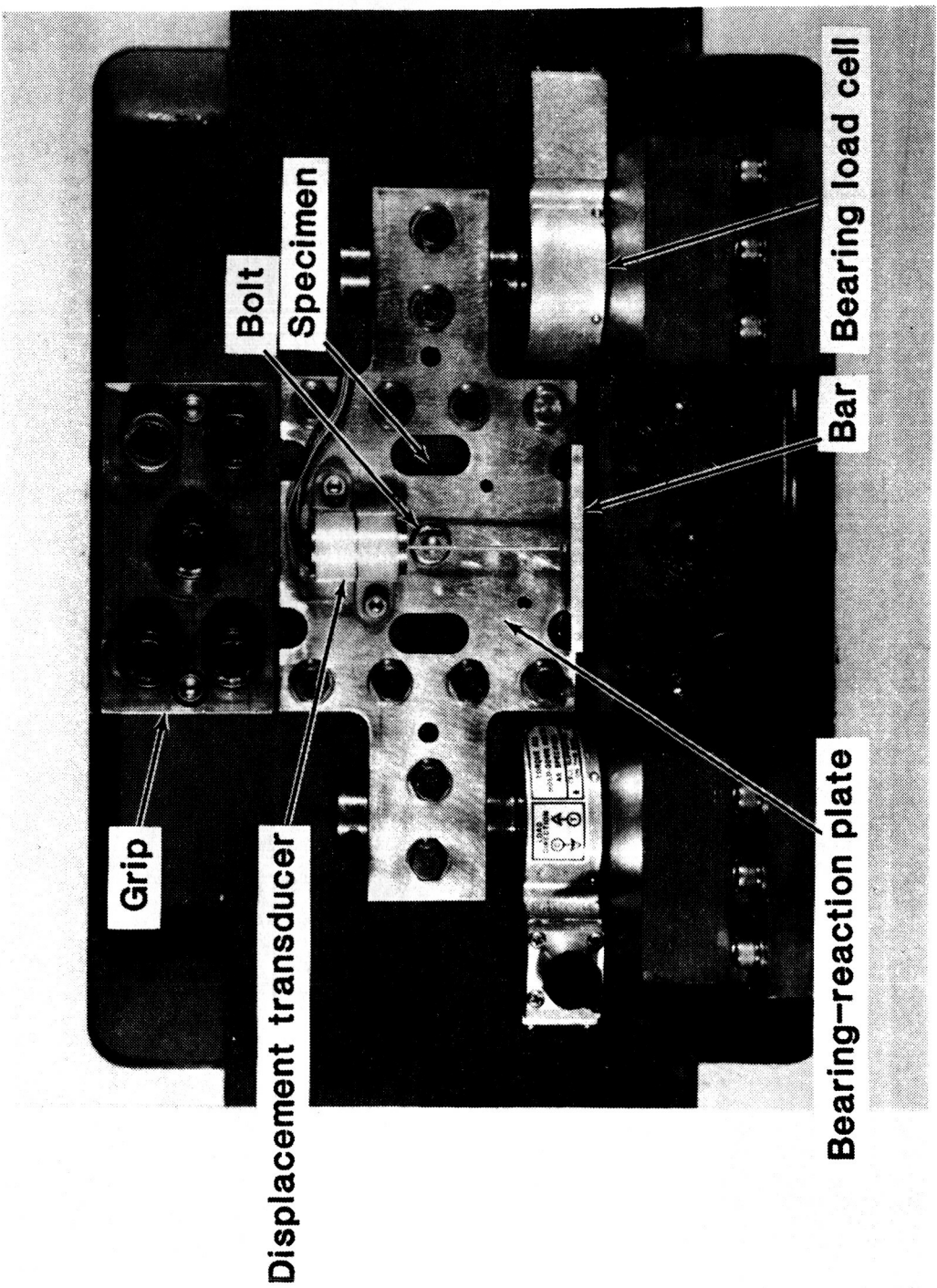


Figure 4 Photograph of bearing-bypass test apparatus.

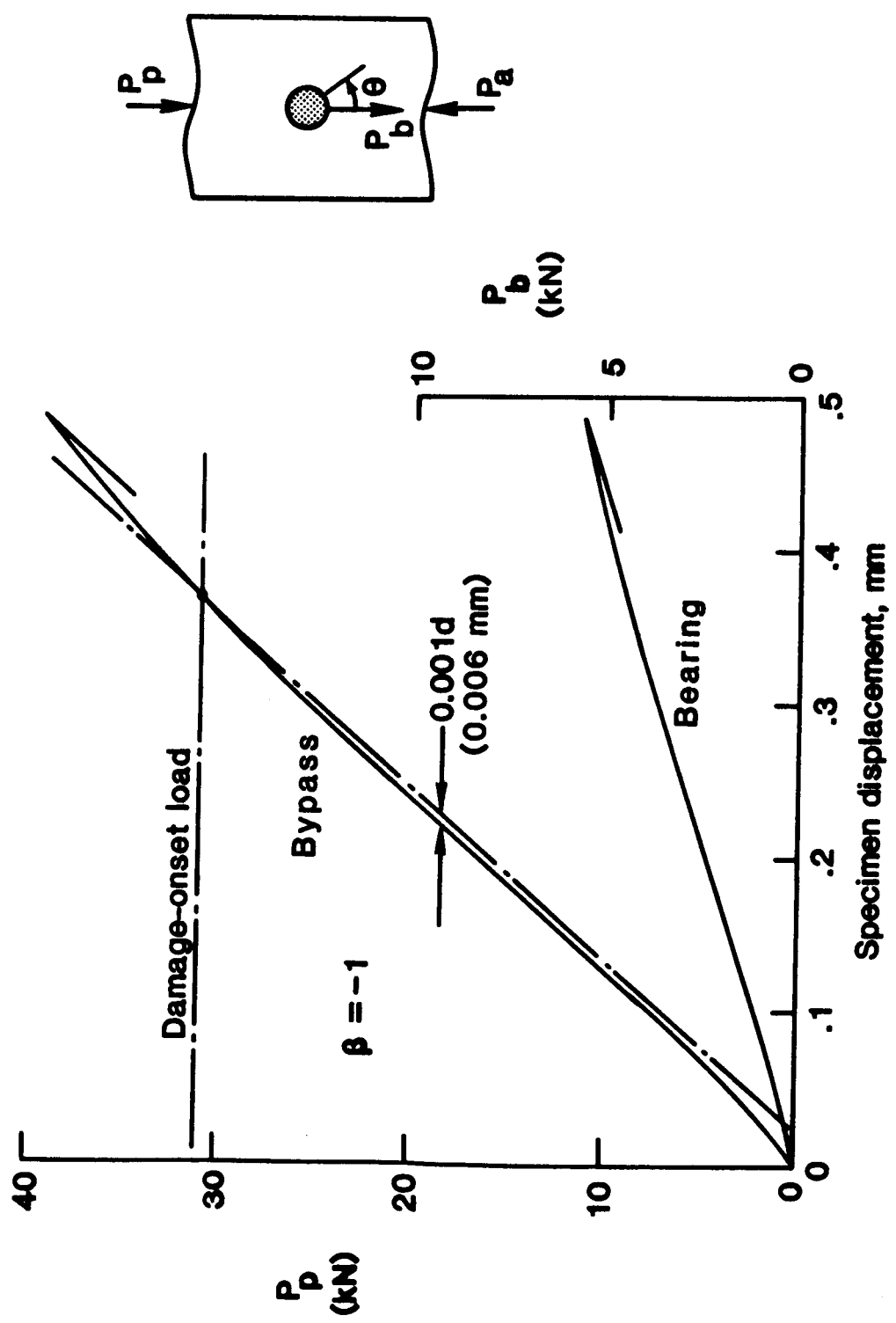
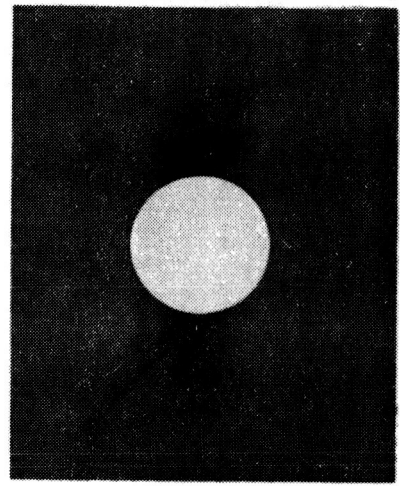
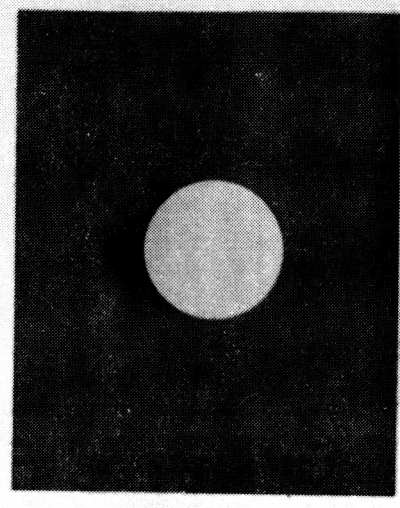


Figure 5 Typical load-displacement curves.

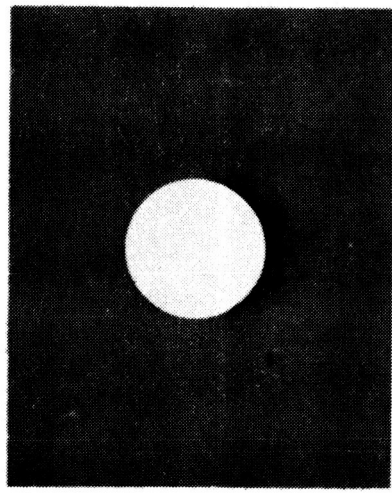
ORIGINAL PAGE IS  
OF POOR QUALITY



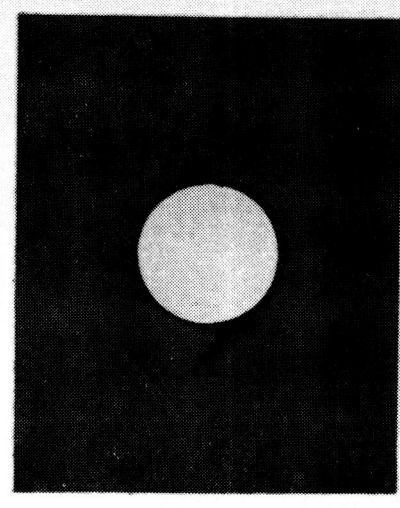
**(a) Net-section tension (NT)**



**(b) Tension-reacted bearing (TRB)**



**(c) Compression-reacted bearing (CRB)**



**(d) Net-section compression (NC)**

Figure 6 Radiographs of damage at fastener hole.

CRB  
OF  
FCB



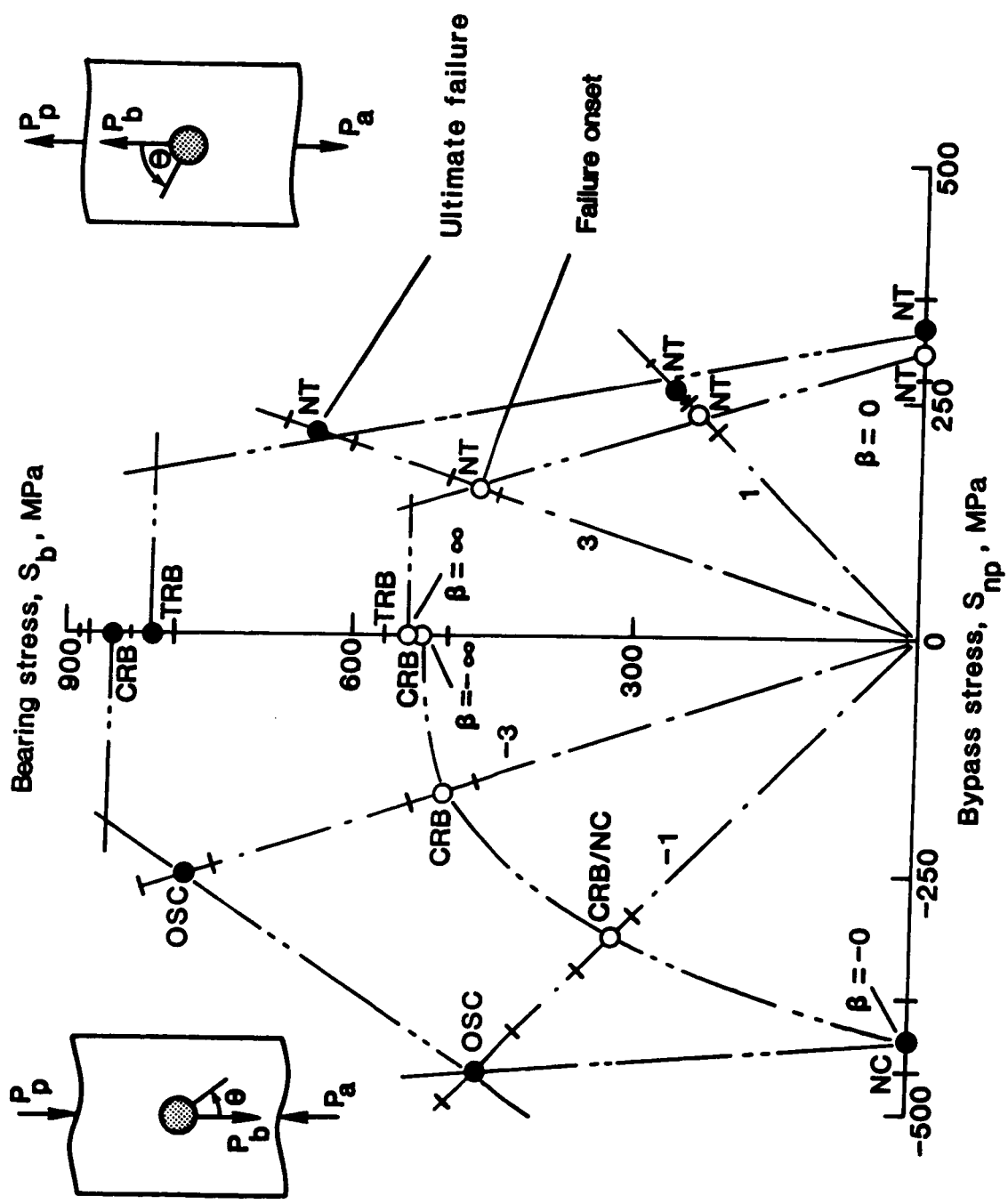


Figure 8 Bearing-bypass diagram for ultimate and damage-onset strengths.

ORIGINAL PAGE IS  
OF POOR QUALITY

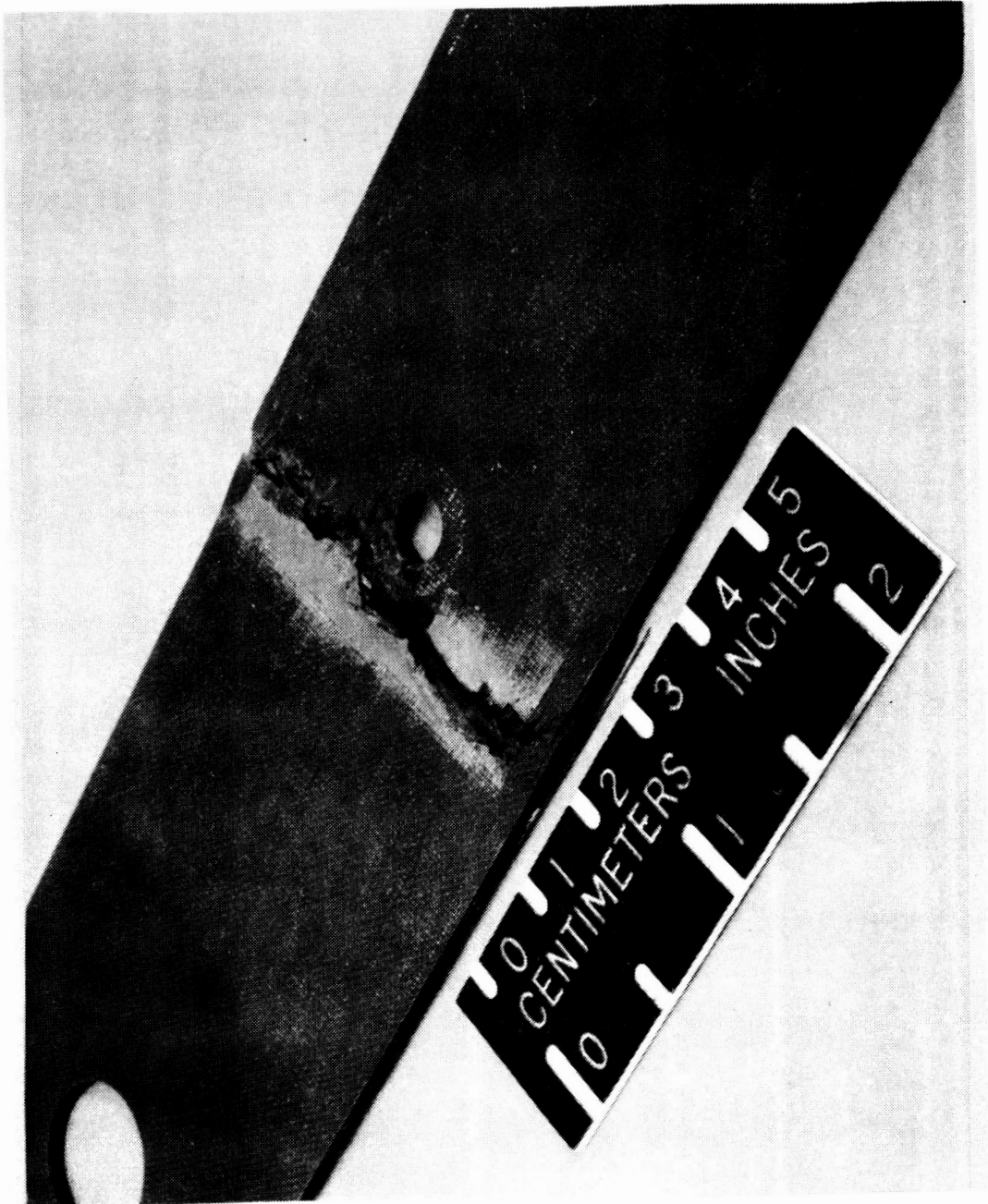


Figure 9 Photograph of a failed specimen showing an offset compression (OSC) failure.

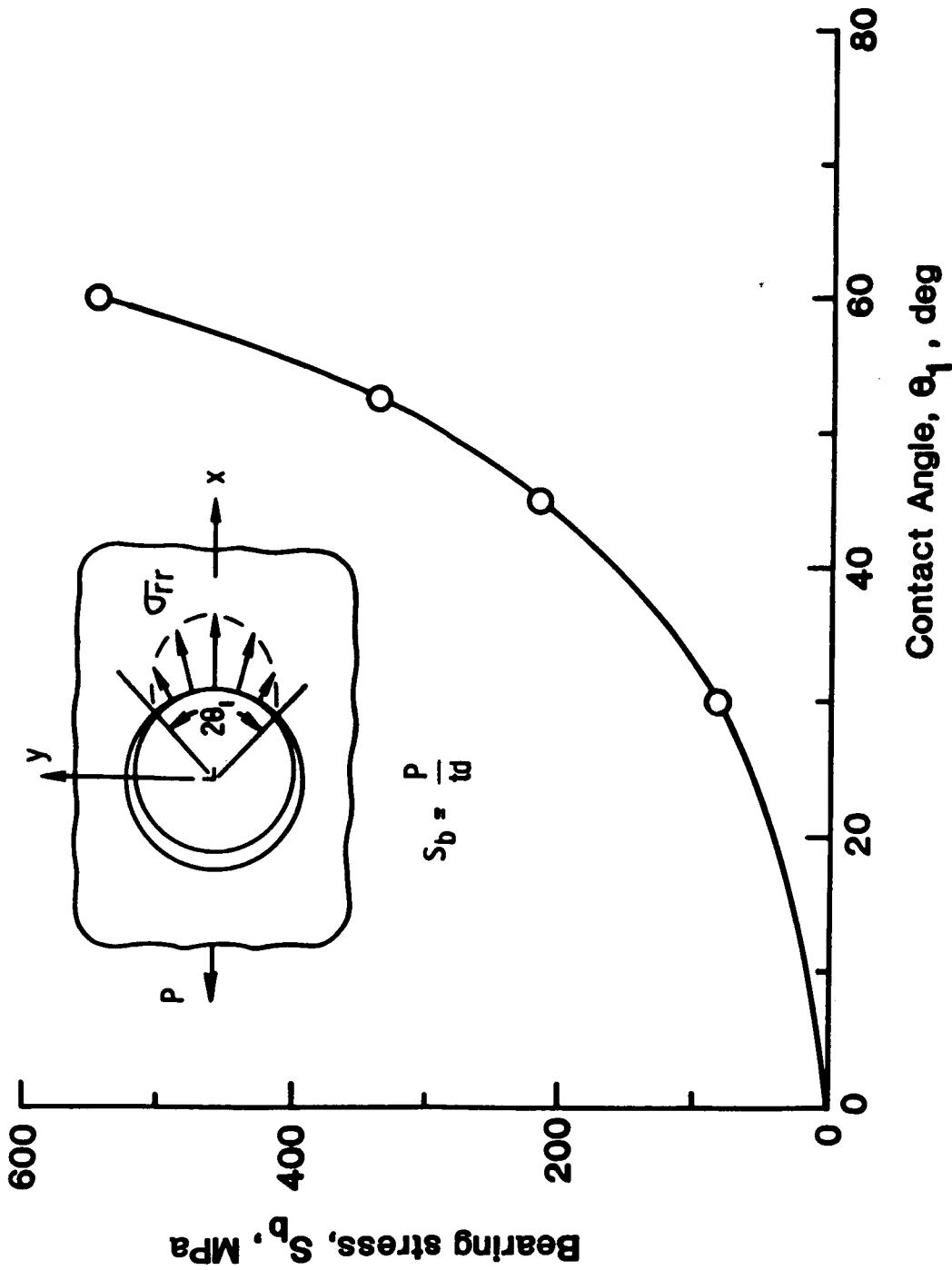


Figure 10 Nonlinear relationship between bearing stress and contact angle.

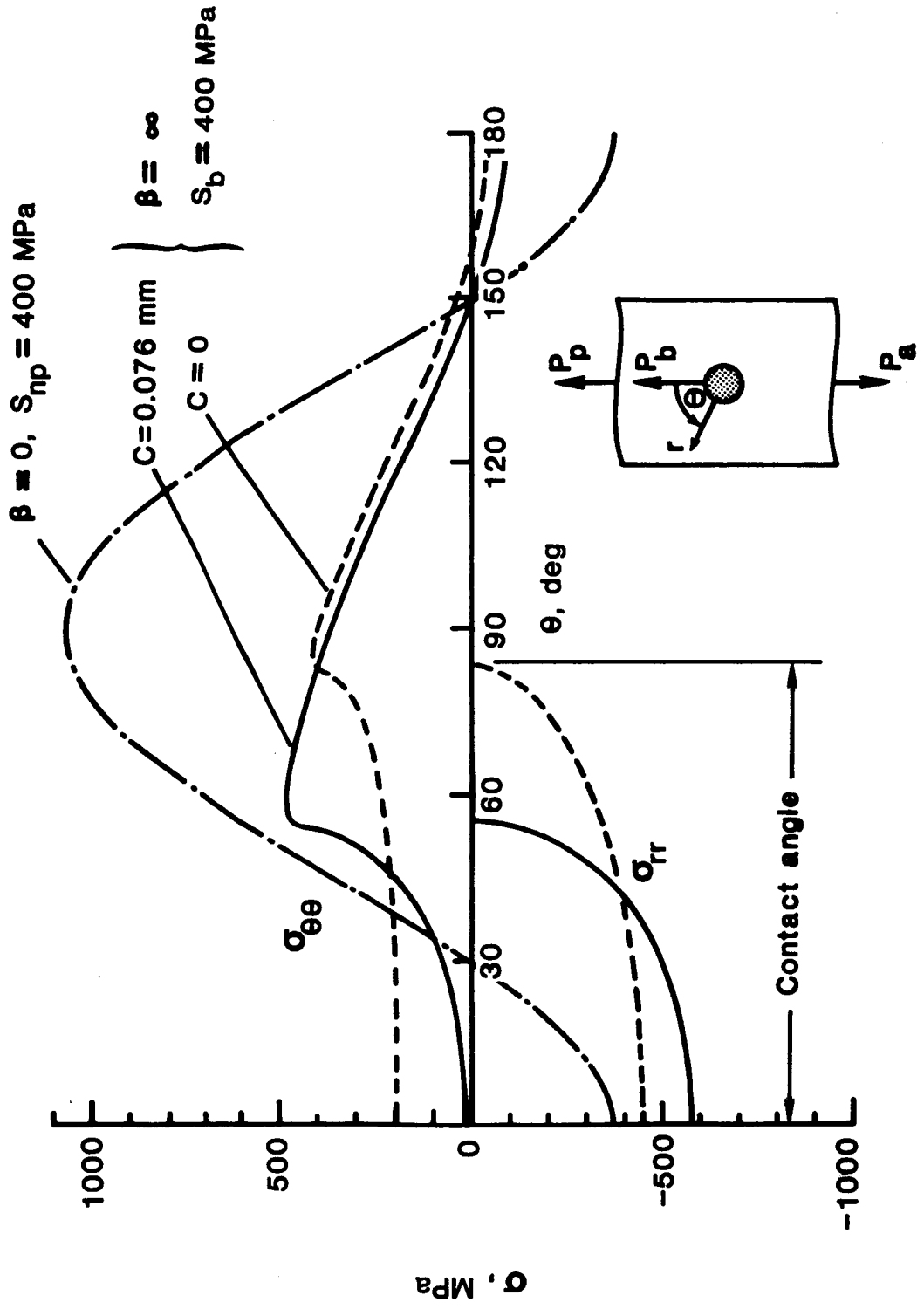


Figure 11 Stress distributions along hole boundary for all bearing and all bypass tension loads.

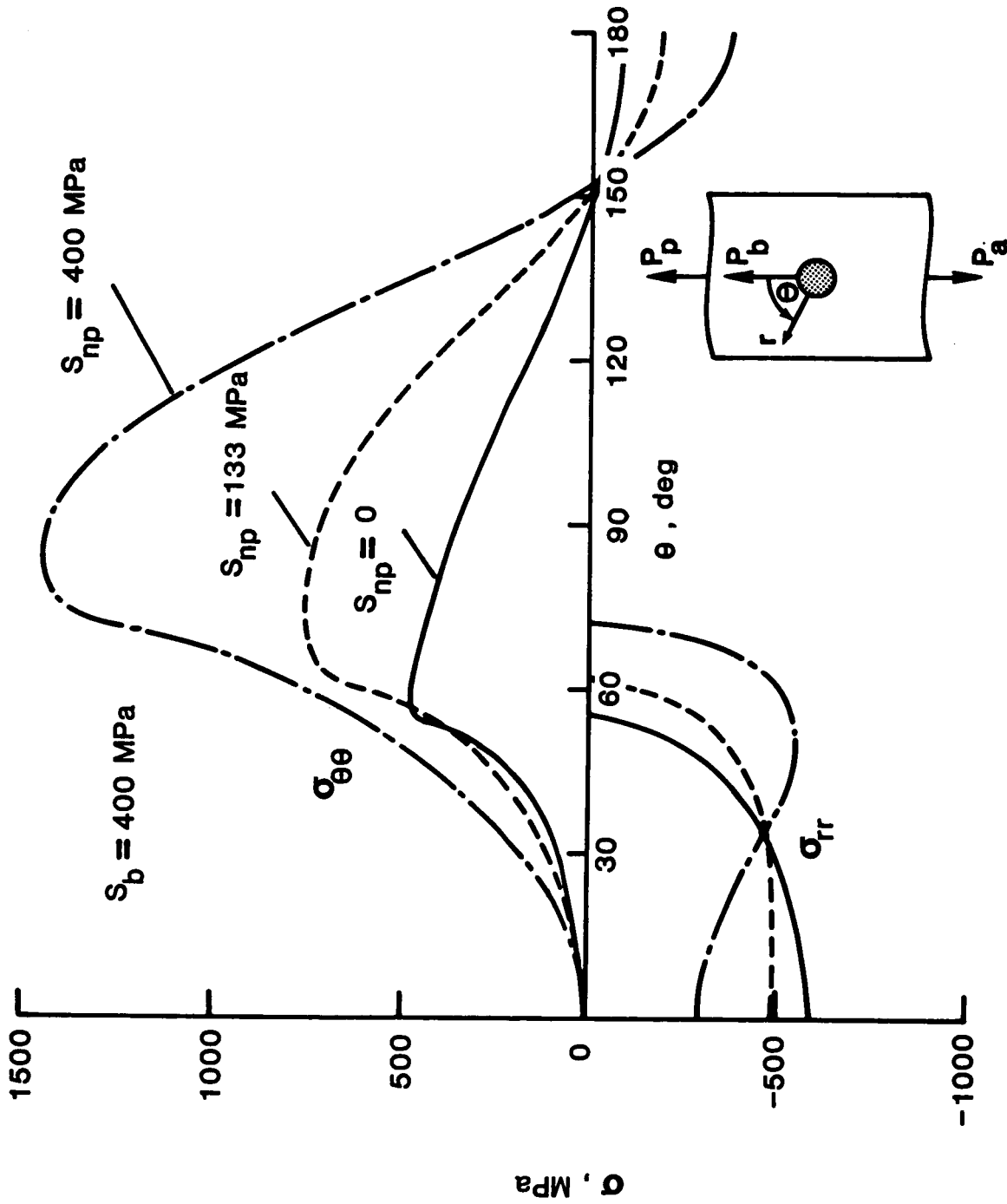


Figure 12 Stress distributions for tension bearing-bypass loadings.

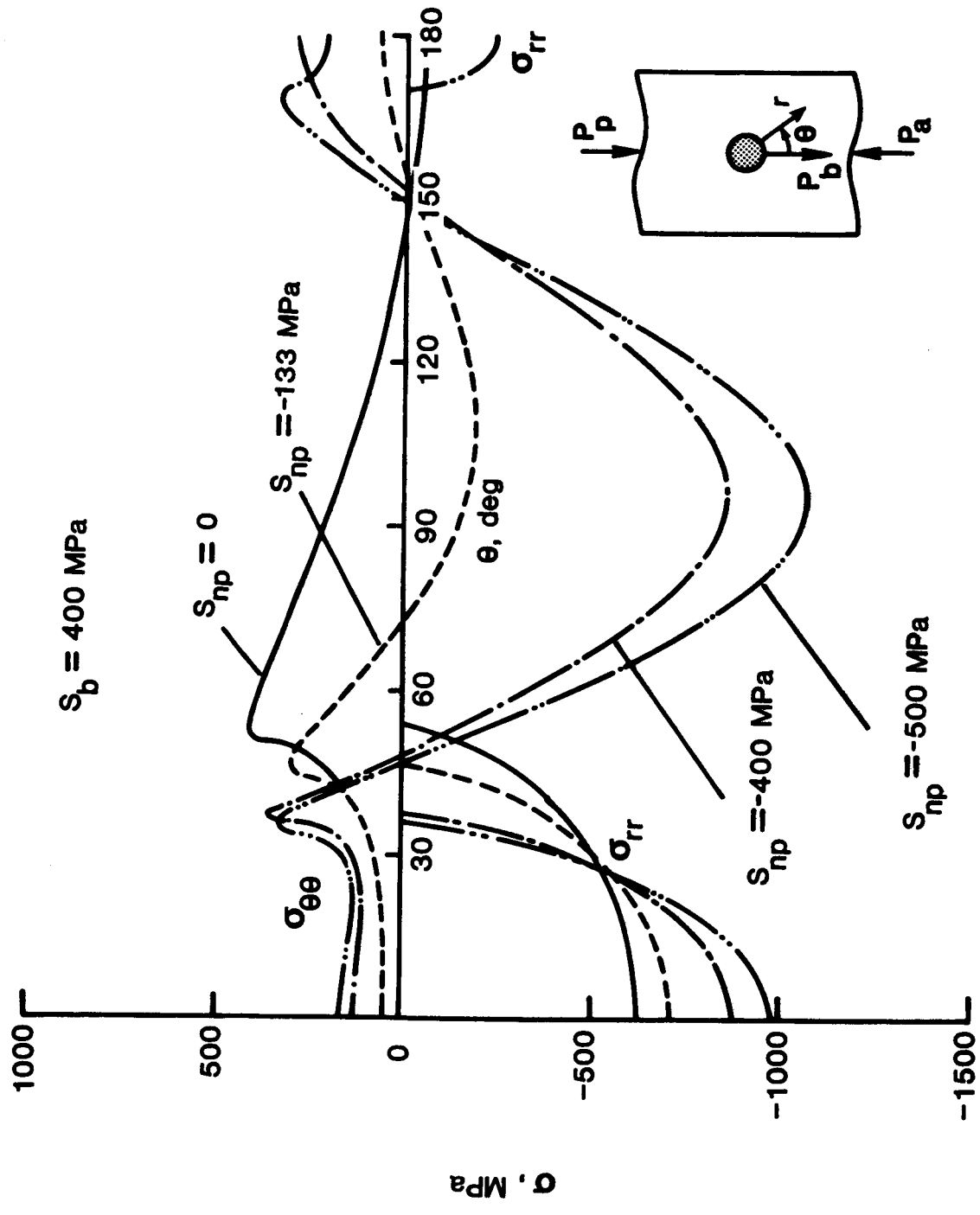


Figure 13 Stress distributions for compression bearing-bypass loadings.

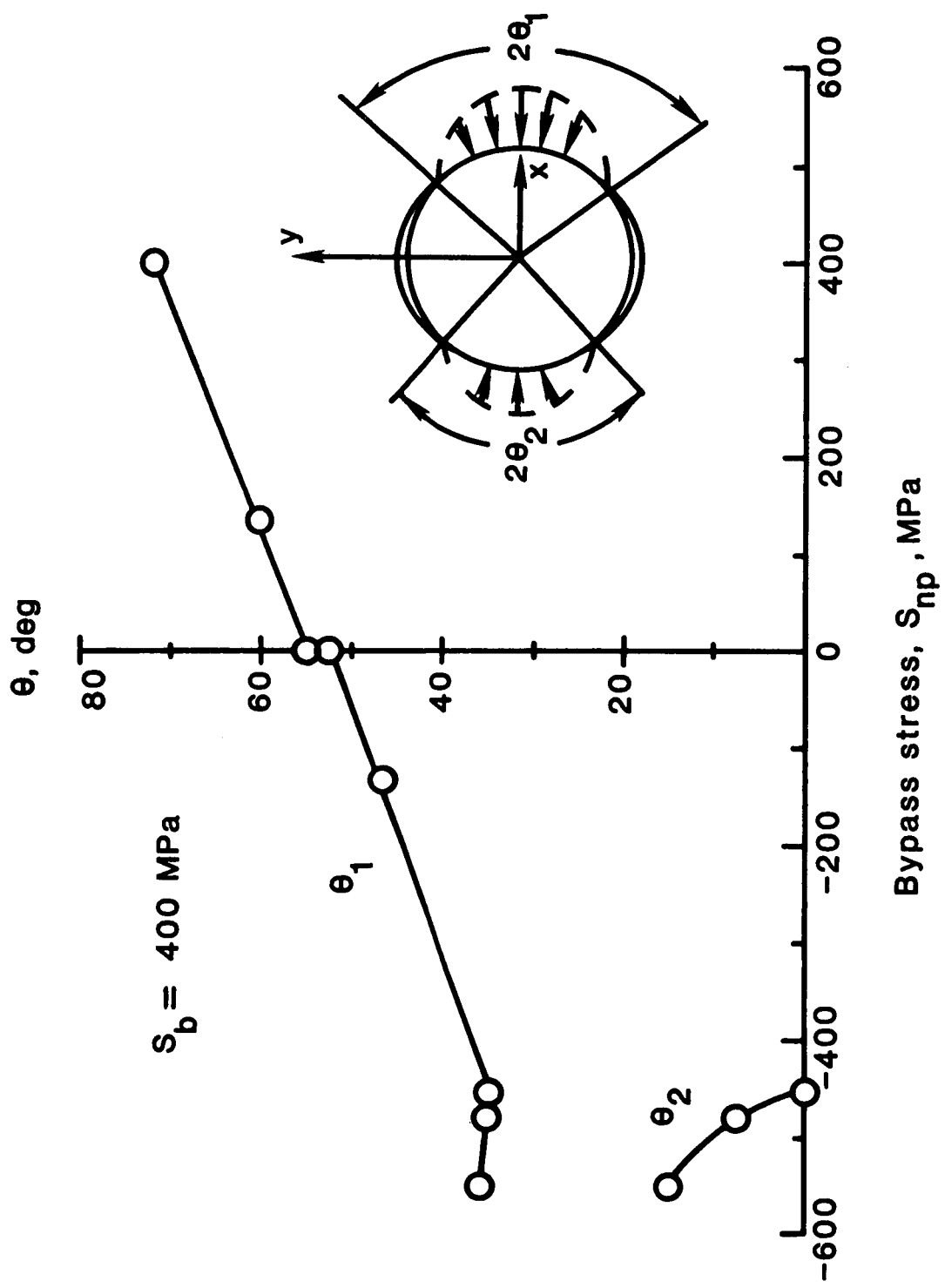


Figure 14 Contact angles for bearing and a range of bypass loadings.

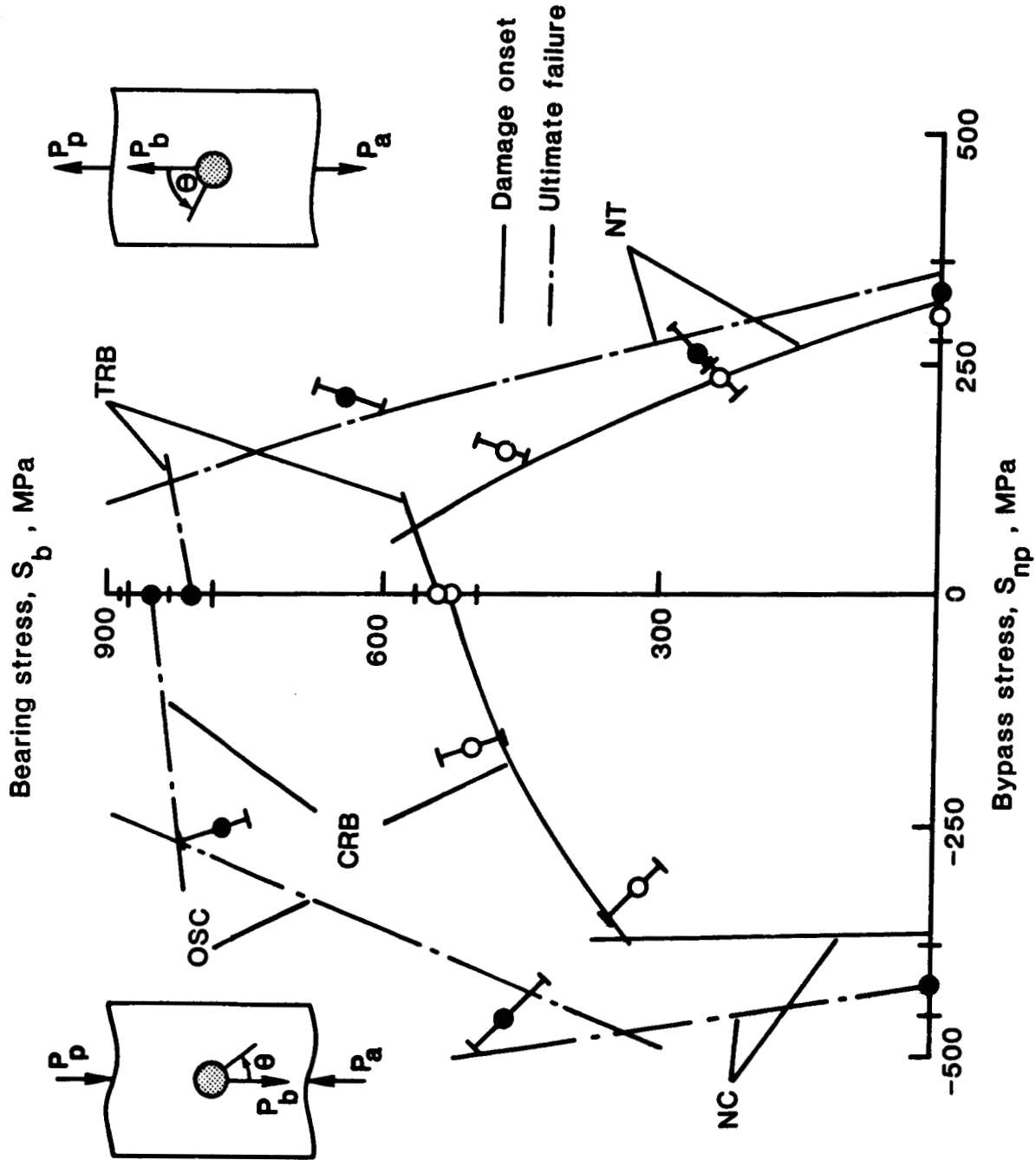


Figure 15 Strength calculations for damage-onset and ultimate failure strengths.

**Standard Bibliographic Page**

1. Report No. <b>NASA TM-89153</b>	2. Government Accession No.	3. Recipient's Catalog No.	
4. Title and Subtitle  <b>Bearing-Bypass Loading on Bolted Composite Joints</b>		5. Report Date <b>May 1987</b>	
		6. Performing Organization Code	
7. Author(s)  <b>J. H. Crews, Jr. and R. A. Naik</b>		8. Performing Organization Report No.	
		10. Work Unit No. <b>505-63-01-05</b>	
9. Performing Organization Name and Address <b>National Aeronautics and Space Administration Langley Research Center Hampton, VA 23665-5225</b>		11. Contract or Grant No.	
		13. Type of Report and Period Covered <b>Technical Memorandum</b>	
12. Sponsoring Agency Name and Address <b>National Aeronautics and Space Administration Washington, DC 20546</b>		14. Sponsoring Agency Code	
		15. Supplementary Notes	
16. Abstract  A combined experimental and analytical study has been conducted to investigate the effects of simultaneous bearing and bypass loading on a graphite/epoxy (T300/5208) laminate. Tests were conducted with a test machine that allows the bearing-bypass load ratio to be controlled while a single-fastener coupon is loaded to failure in either tension or compression. Test coupons consisted of 16-ply quasi-isotropic graphite/epoxy laminates with a centrally-located 6.35-mm bolt having a clearance fit. Onset-damage and ultimate strengths were determined for each test case. Next, a finite element stress analysis was conducted for each test case. The computed local stresses were used with appropriate failure criteria to analyze the observed failure modes and strengths. An unexpected interaction of the effect of the bypass and bearing loads was found for the onset of compression-reacted bearing damage. This interaction was caused by a decrease in the bolt-hole contact arc and a corresponding increase in the severity of the bearing loads. The amount of bolt-hole contact had a significant effect on local stresses and, thus on the calculated damage-onset and ultimate strengths. An offset-compression failure mode was identified for laminate failure under compression bearing-bypass loading. This failure mode appears to be unique to compression bearing-bypass loading and, therefore, cannot be predicted from simple tests.			
17. Key Words (Suggested by Authors(s)) <b>Laminate                      Stress analysis Bolt                              Composites Bearing                         Joint Graphite/epoxy Strength Damage</b>		18. Distribution Statement  <b>Unclassified - Unlimited Subject Category 24</b>	
19. Security Classif.(of this report) <b>Unclassified</b>	20. Security Classif.(of this page) <b>Unclassified</b>	21. No. of Pages <b>33</b>	22. Price <b>A03</b>